# ADVANCES IN FOREST FIRE RESEARCH

## 2022

Edited by
DOMINGOS XAVIER VIEGAS
LUÍS MÁRIO RIBEIRO

# Simulated flame shape and heat transfer of quasi-equilibrium grass fires at transitional Byram numbers

Duncan Sutherland*[1]; Jason Sharples[1], Khalid Moinuddin[2]

*[1]School of Science, UNSW Canberra, Australia, {duncan.sutherland, j.sharples}@adfa.edu.au*
*[3] Institute for Sustainable Industries and Liveable Cities, Victoria University, Australia, {khalid.moinuddin@vu.edu.au}*

**Corresponding author*

**Keywords**

Physics-based simulation, grass fires, quasi-equilibrium spread

**Abstract**

There are two basic modes of fire spread: buoyancy driven where the fire plume is approximately vertical, and wind driven where the fire plume is attached to the surface. The buoyancy driven mode is usually identified by Byram number Nc>10, and the wind driven mode identified by Nc<2. Grass fires at field scale over a range of Byram numbers are simulated using a physics-based model and the mechanisms of heat transfer to the unburnt fuel are analysed. The wind speed is varied to give different Byram number and different fire behaviour. The current thresholds on Byram number are found to correctly classify the behaviour of the fire plume. Previously it was thought that radiative heating dominates convective heating for buoyancy dominated fires, and convective heating dominates radiative heating for wind dominated fires. However, the radiative boundary heat flux is found to dominate the convective boundary heat flux in all cases. The convective heat flux along the centreline ahead of the main fire front increases with wind speed. The results imply that the heat transfer mechanisms, at least for this fire configuration, is more complicated than previously thought. Further research is required to understand if the convective heat transfer mechanisms are adequately reproduced in the simulations.

## 1. Introduction

The Byram convective number $Nc$ (Morvan and Frangieh, 2018) is used in various parts of the literature in an attempt to classify fires as wind-driven (wind-dominated, shear force dominated, or sometimes called the boundary layer mode) or buoyancy-driven (buoyancy dominated, plume driven, or plume mode). In wind-driven fires the flame is elongated and at an acute angle to the ground. Radiative and convective heat transfer to unburnt fuel is thought to be enhanced by the flame geometry. In buoyancy-driven fires the flame is roughly vertical and therefore it is hypothesised that the heat transfer to the unburnt fuel is almost exclusively by radiation (Morvan and Frangieh, 2018). The importance of convective structures and convective heating on fuel ignition and fire spread has been studied experimentally (Finney et al., 2015). The equation for $Nc$ is

$$Nc = \frac{2gQ/(\rho\, c_p\, T_a)}{(U_{10} - R)^3}$$

where $U_{10}$ is the wind speed at 10 m, $Q$ is the fire intensity, $g$ is the acceleration due to gravity, $R$ is the rate of spread, $\rho$ (1.2 kg m$^{-3}$) is the gas density, $c_p$ is the gas specific heat capacity (1.0 kJ kg$^{-1}$ K$^{-1}$ ), and $T_a$ is the ambient temperature. Therefore, the Byram number can be thought of as measuring the relative importance of the buoyant or convective force and the shearing force upon a fire. The thresholds proposed for the Byram number are $Nc < 2$ is a wind-driven fire, $Nc > 10$ is a buoyancy-driven fire, and $2 \leq Nc \leq 10$ is some intermediate fire behaviour.

Physics-based simulations are becoming a popular tool for wildfire investigation. Here we use the Wildland-Urban Fire Dynamics Simulator (WFDS, subversion 9977, based upon FDS version 6.0), which has been validated against field scale fires (Mell et al., 2007, Moinuddin et al., 2018).

Four simulations are conducted, with the driving wind speed the only parameter varied across the simulation set. Specifically, we consider the following wind speed: $U = 3$, 4, 6, and 10 ms$^{-1}$, which are referred to as the

U3, U4, U6, and U10 cases, respectively. The U6 simulation replicates the CO64 experiment conducted during the Annaburoo campaign (Cheney et al., 1993). The rate of spread data for the U3, U6, and U10 cases were presented in (Moinuddin et al., 2018) (averaged quasi-equilibrium value only) and (Sutherland et al., 2020) (values for all time). The Byram number for U3, U6, and U10 at all times was also presented in (Sutherland et al., 2020). All other results, namely the heat transfer and flame shape results, presented here are novel.

## 2. Methodology

WFDS is a fully physics-based fire spread simulator, that is, the solid fuel degradation, gas-phase combustion, heat transfer and fluid flow are explicitly simulated with as few parameterisations as possible. The simulation methodology for grass fire is also well established and the method used here is identical to (Moinuddin et al., 2018, Sutherland et al., 2020).

Several simplifying assumptions are used to model the fuel bed. The fuel is considered as a thin layer on the ground and heat transfer by conduction between the fuel elements is neglected. The fuel dehydrates at 393 K and pyrolyses between 400 and 500 K following a linear mass loss rate [7].

The heat transfer is modelled with several simplifying assumptions. Heat transfer by convection is approximated using an empirical correlation based on approximating the fuels as cylindrical particles. The fuel height and structure are modelled as an aerodynamic drag force term in the fluid momentum equation. The parameters of the convective heat transfer and aerodynamic drag model are deduced from experimental measurements. The flame emits radiation, and the radiation transport equation is solved by the discrete ordinates method. The combustion zone is difficult to resolve using LES, and therefore the gas temperature inside the flame can be underpredicted. Because the emitted radiation depends on the fourth power of gas temperature an underprediction can result in large errors in the radiation term. Therefore, within the flaming zone the source of radiation is a function of local heat release rate per unit volume. Outside the flaming zone, gas temperature is well resolved and the usual fourth power of temperature relation is used. Full details of the WFDS model can be found in (Mell et al., 2007).

## 3. Results and discussion

### 3.1. Quasi-equilibrium fire spread

The contours of burning area over time, are extracted from the boundary temperature, $T$, data. The $T = 400$ K contour at time $t$ represents the extent of the burning region.

The burnable region of the simulation domain and example fire isochrones for the U4 case, are shown in Figure 1.

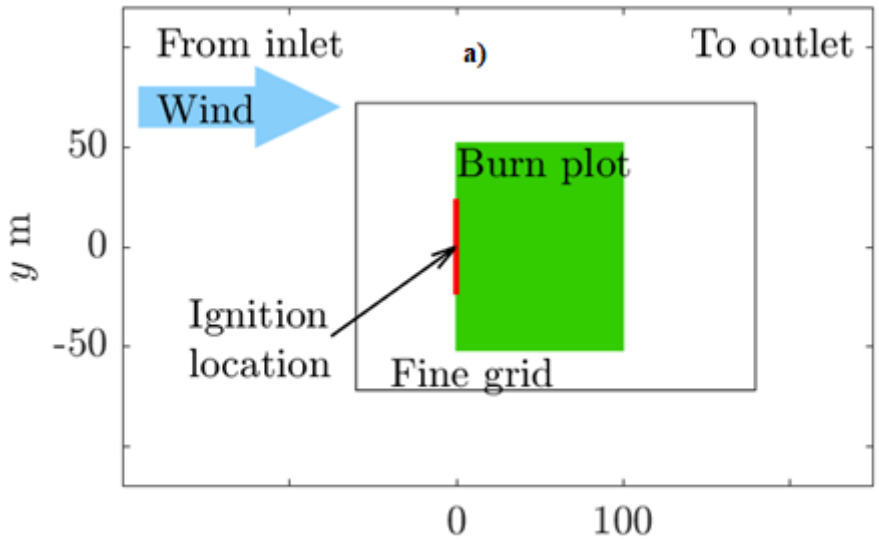

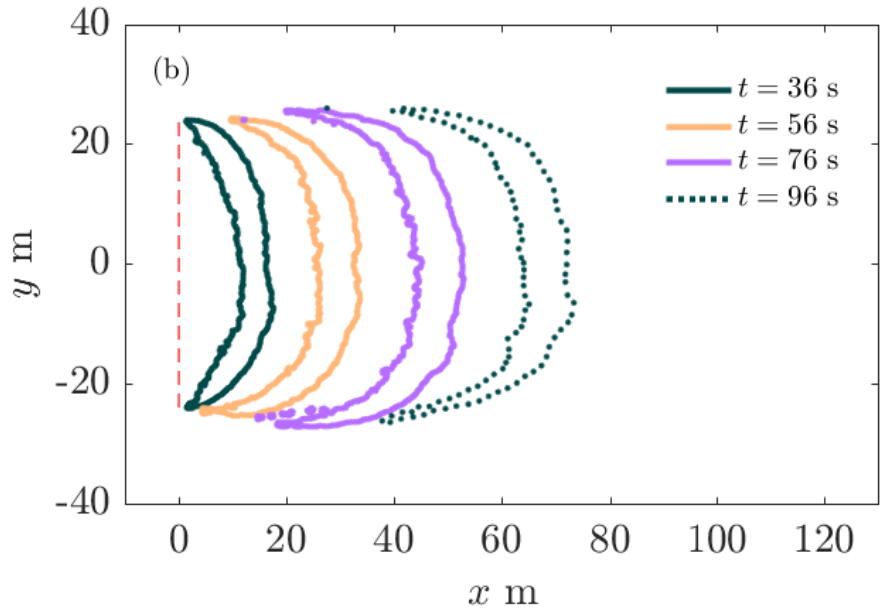


***Figure 1- (a) a schematic of the simulation (b) example fire isochrones for the U4 case.***

The rate of spread of the fire is estimated from the boundary temperature along the domain centreline. The location of the burning region, $x_*$ is identified from the centre of the interval along $y = 0$ where $T_s > 400$ K. The time dependent rate of spread is then the time derivative of $x_*$; the derivative is approximated from the simulation data using the standard first-order forward difference scheme:

$$\mathrm{R(t)} = \frac{dx_*}{dt} \approx \frac{\mathrm{x_*(t_{n+1})} - \mathrm{x_*(t_n)}}{t_{n+1} - t_n}$$

The time interval between the data points is 1 s.

Because the data is noisy, the results are smoothed by a 5-point moving average. The quasi-equilibrium rate of spread $R_{qe}$ is then judged manually from the region where $R(x_*)$ is approximately constant. $R(x_*)$ is shown for the quasi-equilibrium regions for all cases in Figure 2(a). Plotting against location stretches $R(t)$ for the higher speed cases to provide a consistent abscissa and allow easier comparison between the different wind speed cases. $R_{qe}$ is achieved at different times for different driving wind speeds. However, the distance from ignition at which a fire can be deemed quasi-equilibrium is approximately the same: 50 m, which is the threshold used here. $R(x_*)$ decreases rapidly from approximately $x_* = 95$ m as the fire reaches the end of the plot, and these data are omitted from the plots and subsequent analysis. Figure 2(b) shows the corresponding Byram numbers.

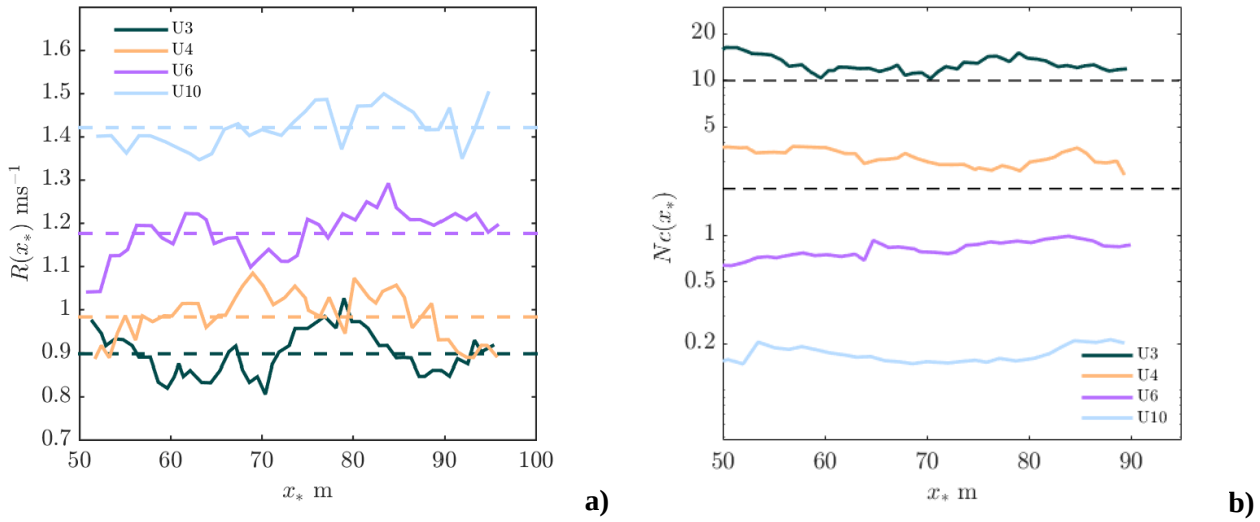


***Figure 2- (a) Rate of spread as a function of distance from the ignition line, in the quasi-equilibrium range. (b) the Byram number. The black dashed lines indicate the threshold limits of Nc=2 and Nc=10.***

### 3.2. Quasi-equilibrium flame shape

Because the fires spread at a quasi-equilibrium rate, and the head fire geometry is approximately constant during this phase of spread, ensemble averages of pyrolysis front, boundary radiative heat flux, boundary convective heat flux, centreline heat release rate, and centreline wind velocities can be constructed in a reference frame that moves with the fire. Similar ideas were used by Mueller (2107) to analyse flame geometry.

To construct the ensembles, all data outside of the quasi-equilibrium region were discarded. The trailing edge of the fire was selected as the reference point. At each output step the data was circularly shifted such that the reference point was located at $x = 0$. That dataset was then averaged in time. Errors are introduced by the circular shift; however, these occur far upstream ($x < -100$ m) and far downstream ($x > 100$ m) and can be discarded.

The ensemble averaged $u$-velocity contours (shaded colours) and the contour of 10% of maximum heat release rate (red) are shown in Figure 3. The red contours were selected as a representation of the flame shape: most of the heat released by the flame is on the inside of this contour. The white arrows in the plot are vector representation of the ensemble averaged $u$- and $v$-velocities. In the U3 case, the $u$-velocity is negative on the downstream side of the flame. To highlight this, the $u = 0$ contour is shown in black. This, and the velocity vector field (white arrows), indicates that the flame and plume entrain fresh air from both sides and is therefore truly a buoyancy dominated fire, consistent with the Byram number prediction. No other cases exhibit two-sided entrainment into the plume. The U4 and U6 cases exhibit roughly vertical flames like the U3 case. The U4 and U6 case exhibit downstream enhancement of the $u$-velocity, however, this is more prominent in the U6 case. In the U4 case the velocity enhancement decays after approximately 25 m but the enhancement persists for at least 50 m in the U6 case. This suggests that the plume of the U6 case has attached to the ground and this attachment persists for some distance. The plume attachment is consistent with the Byram number prediction of a wind dominated fire. The U4 case has an intermediate Byram number, although with $Nc \approx 3.26$ this fire is notionally closer to wind dominated than buoyancy dominated. The single sided entertainment is consistent with a wind dominated fire, but the $u$-velocity enhancement does not persist for significant distances, suggesting that the plume has detached close to the flaming region. The U10 case shows an elongated heat release rate contour and significant downstream enhancement of the $u$-velocity; consistent with a wind dominated fire.

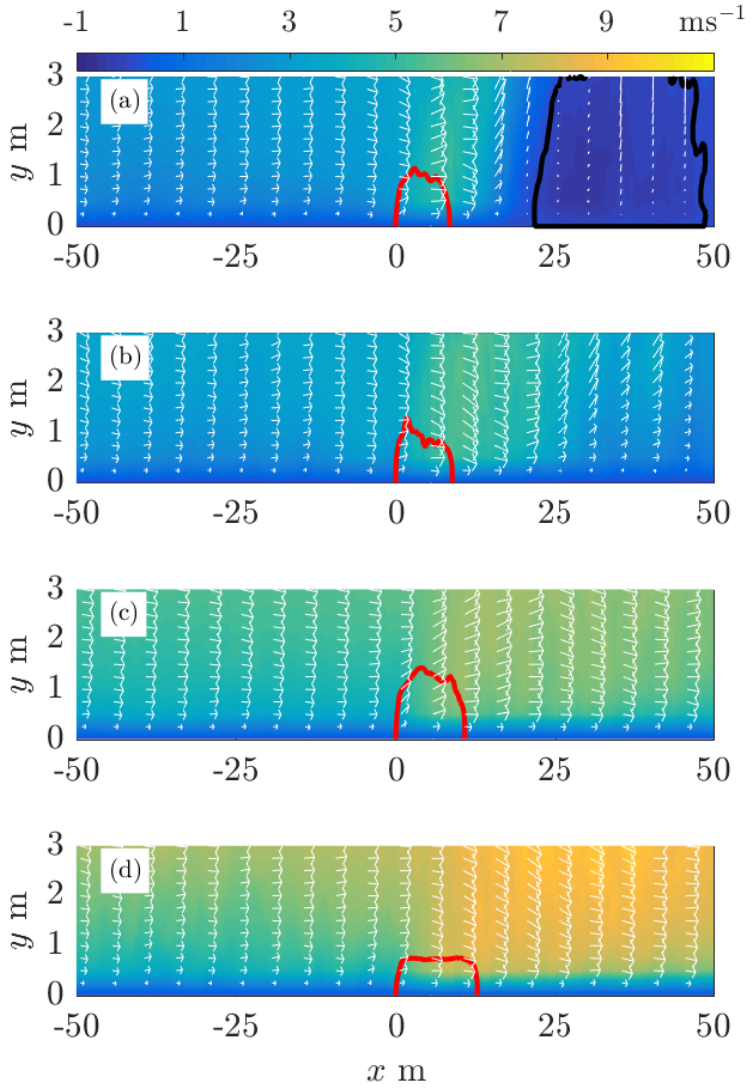


***Figure 3- Contours of 10% of maximum heat release rate (red) per unit volume along the line y = 0 averaged in time over the quasi-steady regime superposed on colour contour plot of averaged u−velocity (a) U3 case (b) U4 case (c) U6 case (d) U10 case. To to highlight the region of negative u−velocity in the U3 case, the u = 0 contour is plotted in black. The white arrows show the direction of the ensemble averaged wind field along the centreline***

### 3.3 Analysis of heat transfer

To investigate how the mechanisms of heat transfer change with the mode of fire propagation, the total radiative and convective heat fluxed received by the unburnt fuel is computed. However, the data may still include cooling of the unburnt fuel by radiation and convection, and such cooling is expected at the flanks and trailing edge regions of the fire. To examine the regions of heat transfer, the contours of ensemble-averaged boundary (z=0 m) heat flux are shown in Figure 4 (radiative) and Figure 5 (convective).

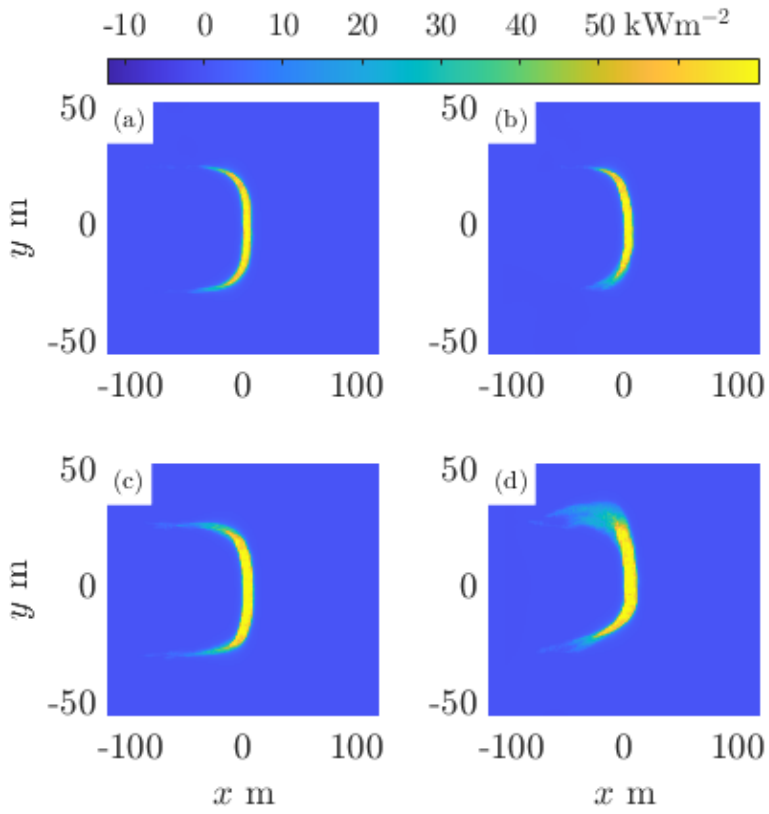


***Figure 4- Ensemble averaged radiative heat transfer (a) U3 (b) U4 (c) U6 (d) U10***

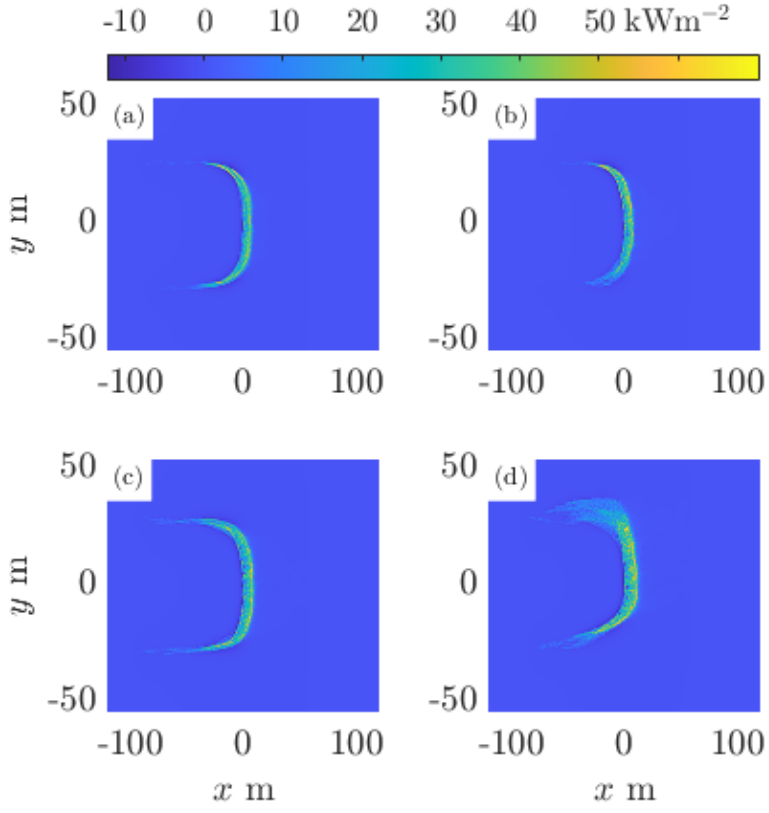


***Figure 5 Ensemble averaged convective heat transfer (a) U3 (b) U4 (c) U6 (d) U10***

The shape of the contour is like the shape of the pyrolysis zone. The heat fluxes are most intense in the straighter near-centreline head region of the fire. However, at the edges and trailing regions of the fire, the averages appear

indistinct. This phenomenon is strongest around $y = 40$ m in the U10 case. The flanks of the fires, unlike the near centreline behaviour of the fires, are somewhat intermittent and cannot be in a quasi-equilibrium state.

There is little to no radiative cooling, however, there is strong evidence of convective cooling, located at the trailing edge of the fire. The variation in the convective heat flux across the head fire may be associated with the vortex structures identified by Finney et al. (2015). Because these structures appear in the ensemble average, these structures must persist in approximately the same y-location over the quasi-equilibrium propagation.

To identify if there is a dominant mechanism of heat transfer along the centreline, the ensemble averaged boundary heat fluxes are shown upon the centreline in Figure 6. The vertical dotted lines are the locations of the leading edge of the heat release rate contour shown in Figure 3. The centreline radiative heat flux exhibits a single broad peak, which stretches in the positive $x$-direction as $U$ increases. The centreline convective heat flux has a more complicated shape. There is a region of cooling before the trailing edge, followed by a peak in heating at the trailing edge ($x = 0$ m). The magnitude of the cooling and heating peaks are similar for all wind speeds. There is a region of decreased heat transfer at approximately $x = 2$ m, even extending to a region of cooling in the U10 case. The magnitude of this trough does not appear to follow a systematic trend. It is possible that this region is associated with the previously identified vortex structures that occurs near the centreline in all cases.

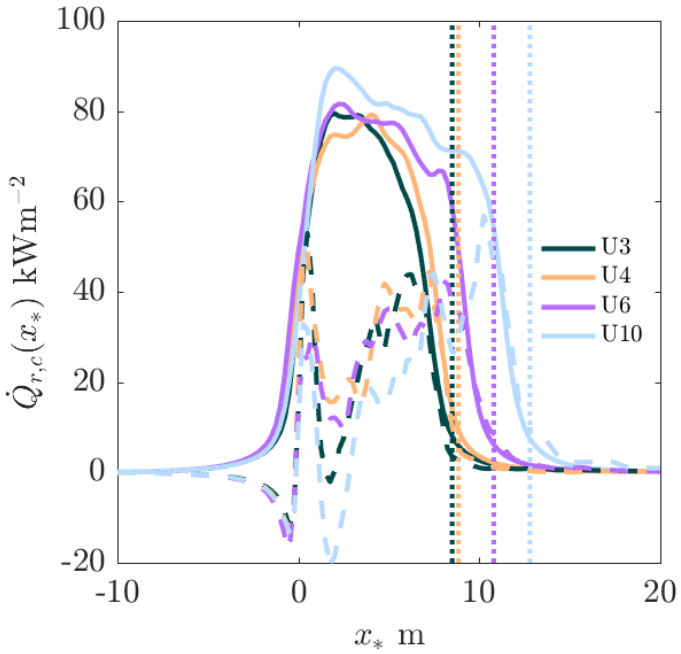


***Figure 6- Centreline radiative (solid) and convective (dotted) heat transfer to the unburnt fuel. The vertical dotted lines are the leading edge of the heat release contour shown in Figure 3.***

The main peak convective heat flux does increase and stretch in the positive $x$-direction like the radiative heat flux. The U10 case has a peak of convective heat flux of similar magnitude to the value of radiative heat flux at $x = 10$ m. Similar trends are observable at lower velocities. Therefore, it appears that at the leading edge of the fire, for these cases, both centreline radiative and convective heat fluxes are of approximately equal magnitude. The convective heat flux in the U10 case exceeds the radiative heat flux at $x \approx 15$ m, consistent with the observations of Finney et al. (2015). However, Finney et al. do not look directly at convective heat flux in the flaming region, as we have done. Instead, they observe particle temperature ahead of the main fire front and infer the behaviour of the convective heat flux. The simulated convective heat flux is $\dot{q}'' = h\,(T_w - T_g)$ where $h$ is the convective heat transfer coefficient based upon natural and forced convection empirical correlations. The $T$ with subscripts $w$ and $g$ represent the wall (fuel) and gas temperature respectively. WFDS has been validated by comparing the simulated rate-of-spread to observations (Mell et al. 2007, Moinuddin et al. 2018) however, there is little direct (i.e. measuring and simulating fuel temperature ahead of the front) validation for the convective heat transfer model in surface grass fires and further research is required to investigate the heat transfer further.

## 4. Conclusions

The Byram number correctly predicts the plume dynamics as expected. Low $Nc$ cases have elongated and attached flames with one-sided entrainment into the plume; whereas higher $Nc$ cases have a more vertical flame with two-sided entrainment.

For these simulations, the dominant heat transfer mechanism was found to be radiation in all cases. The radiative heat transfer was always approximately twice as much as the convective heat transfer, even if the flame was attached in a wind dominated fire. On the centreline, considered representative of the head fire behaviour, convective heating emerges to be of approximately equal magnitude as radiative heating at the leading edge of the fire. This is contrary to the hypothesis that convective heating takes over as the dominant mechanism of heat transfer in wind driven cases. While the results presented here are specific to this fire geometry and represent only a relatively small window of near transitional $Nc$, the hypothesised behaviour of heat transfer mechanisms are likely more complicated than currently thought and understood.

## 5. References

Morvan, D., & Frangieh N., Wildland fires behaviour: wind effect versus Byram's convective number and consequences upon the regime of propagation, International Journal of Wildland Fire 27 (9) (2018) 636–641

Finney, M. A., Cohen, J. D., Forthofer, J. M., McAllister, S. S., Gollner, M. J., Gorham D. J., Saito, K., Akafuah, N. K., Adam, B. A., & English, J. D., Role of buoyant flame dynamics in wildfire spread, Proceedings of the National Academy of Sciences 112 (32) (2015) 9833–9838.

Mell, W., Jenkins, M., Gould, J., & Cheney, P., A physics-based approach to modelling grassland fires, International Journal of Wildland Fire 16 (1) (2007) 1–22

Moinuddin, K. A. M., Sutherland, D., & Mell, W., Simulation study of grass fire using a physics-based model: striving towards numerical rigour and the effect of grass height on the rate-of-spread, International Journal of Wildland Fire 27 (12) (2018) 800–814

Cheney P., Gould, J., & Catchpole, W., The influence of fuel, weather and fire shape variables on fire-spread in grasslands, International Journal of Wildland Fire 3 (1) (1993) 31–44

Sutherland, D., Sharples, J. J., Moinuddin, & K. A. M. The effect of ignition protocol on grassfire development, International journal of wildland fire 29 (1) (2020) 70–80

Morvan, D., & Dupuy, J., Modeling the propagation of a wildfire through a Mediterranean shrub using a multiphase formulation, Combustion and flame 138 (3) (2004) 199–210.

Mueller, E. V., Examination of the underlying physics in a detailed wildland fire behavior model through field-scale experimentation (2017) PhD Thesis, University of Edinburgh.